Building a Better B-Dot: Fast Detumbling with Non-Monotonic Lyapunov Functions

Jacob B. Willis
Robotics Institute
Carnegie Mellon University
5000 Forbes Ave.
Pittsburgh, PA 15213
jbwillis@cmu.edu

Paulo R.M. Fisch
Robotics Institute
Carnegie Mellon University
5000 Forbes Ave.
Pittsburgh, PA 15213
pfisch@andrew.cmu.edu

Aleksei Seletskiy
Robotics Institute
Carnegie Mellon University
5000 Forbes Ave.
Pittsburgh, PA 15213
aseletsk@andrew.cmu.edu

Zachary Manchester
Robotics Institute
Carnegie Mellon University
5000 Forbes Ave.
Pittsburgh, PA 15213
zacm@cmu.edu

Abstract—**Spacecraft detumbling with magnetic torque coils is an inherently underactuated control problem. Contemporary and classical magnetorquer detumbling methods do not adequately consider this underactuation, and suffer from poor performance as a result. These controllers can get stuck on an uncontrollable manifold, resulting in long detumbling times and high power consumption. This work presents a novel detumble controller based on a non-monotonic Lyapunov function that predicts the future magnetic field along the satellite's orbit and avoids uncontrollable configurations. In comparison to other controllers in the literature, our controller detumbles a satellite in significantly less time while also converging to lower overall angular rates. We provide a derivation and proof of convergence for our controller as well as Monte-Carlo simulation results demonstrating its performance in representative use cases.**

Table of Contents

1. Introduction

After a spacecraft is deployed on orbit, a common first phase of operation is detumbling. In this phase, the angular velocity of the satellite is reduced from tens of degrees per second to rates that are tolerated by the satellite mission or managed by other onboard control systems. To perform detumbling, the spacecraft must reduce its total angular momentum by one-to-two orders of magnitude. This is only accomplished by generating external torques, either through expending propellant, or, in low-Earth orbit, with magnetic torque coils (magnetorquers) that exchange momentum with the Earth's magnetic field.

Magnetorquers are appealing because they do not require expending propellant. However, magnetorquers are underactuated: at any instant in time, they only generate torque in a two-dimensional subspace perpendicular to the Earth's local magnetic-field vector. To prove convergence, most common magnetorquer detumbling controllers, including the classic B-dot and B-cross controllers [1], [2], rely on the motion of the satellite through the Earth's magnetic field, which makes the magnetic field vector time varying in the orbit frame. While instantaneously underactuated, over the spacecraft's full orbit, full controllability is achieved. In this work, we demonstrate that these classic controllers, and their modern variants, can take many hours to detumble a spacecraft, despite it being possible to detumble much faster and with much less total control effort. For this reason, these controllers are inefficient, wasting precious energy and time during the critical early stages of satellite operation.

To mitigate the inefficiencies of the classic magnetic detumbling controllers, we present a novel controller that uses a prediction of the future magnetic field vector, dramatically improving convergence time. The magnetic field prediction is done using only gyroscope and magnetometer sensor measurements; no inertial attitude or position reference is required. The controller is based on a discrete-time non-monotonic Lyapunov function [3], which is able to temporarily increase the angular momentum of the spacecraft, allowing the system to move away from control singularities. We compare our controller against controllers in the literature using a Monte-Carlo simulation of 100 randomly sampled initial conditions. Our controller detumbles a satellite in half the time of other controllers; it also converges to lower overall angular rates.

Our contributions include:
- A unified treatment of the numerous magnetorquer detumbling controllers that exist in the literature
- A derivation and analytic proof of convergence of our predictive detumbling controller based on a discrete-time non-monotonic Lyapunov function
- Monte-Carlo simulation experiments showing the performance of our predictive controller in comparison to five other controllers in the literature

The paper proceeds as follows: In Section 2 we discuss prior work on magnetorquer detumbling. In Section 3 we present the attitude dynamics of a spacecraft and provide a

unified derivation of the five detumbling controllers that we compare ours to. We also provide a brief introduction to non-monotonic Lyapunov functions. In Section 4 we derive our discrete-time non-monotonic detumbling controller, and in Section 5 we present our Monte-Carlo simulation results. Finally, we summarize our conclusions and suggest directions for future work in Section 6.

2. RELATED WORK

Magnetorquer detumbling has a long history dating back to the earliest days of space exploration [1], [4]. In general, magnetorquer detumbling controllers come in two categories with many variants: B-dot and B-cross. B-dot controllers assume only magnetometer measurements are available. B-cross [2], [5] controllers assume both magnetometer and gyroscope measurements are available onboard the spacecraft. As we will show in Section 3, these two categories are related by a simple approximation, and the many variations in the literature reduce to a variety of gains and saturation methods for handling control limits [6], [7], [8].

In addition to the magnetic detumbling methods discussed here, there has been significant work on full magnetic attitude control, including the work by Wisniewski [9] which models the magnetic field as a periodic system, and more recent work that utilizes numerical optimal control to perform three-axis magnetorquer attitude control [10], [11]. Ovchinnikov presents a recent survey of both magnetorquer detumbling and attitude control [12].

3. BACKGROUND

Attitude Dynamics

Let $h \in \mathbb{R}^3$ be the angular momentum of a spacecraft, $B \in \mathbb{R}^3$ be the Earth's local geomagnetic field vector at the spacecraft's location, and $\mu \in \mathbb{R}^3$ be the dipole moment produced by the spacecraft's magnetorquers.

With a magnetic dipole moment as input, a spacecraft's angular momentum dynamics expressed in an inertial reference frame are

$$\dot{h} = \tau = -B \times \mu = -\hat{B}\mu \qquad (1)$$

where $\tau \in \mathbb{R}^3$ is the torque on the spacecraft and $\hat{B}$ is the skew-symmetric cross product matrix,

$$\hat{B} = \begin{bmatrix} 0 & -B_z & B_y \\ B_z & 0 & -B_x \\ -B_y & B_x & 0 \end{bmatrix}. \qquad (2)$$

With inertia matrix $J \in \mathbb{R}^{3 \times 3}$, the angular momentum relates to the angular velocity as

$$h = J\omega. \qquad (3)$$

We make use of the time derivative of the geomagnetic field vector with respect to the spacecraft's body frame, $\dot{B}^{\mathcal{B}}$, and with respect to the inertial frame, $\dot{B}^{\mathcal{N}}$. Both are expressed in body-fixed coordinates. The relationship between these quantities is

$$\dot{B}^{\mathcal{N}} = \hat{\omega}B + \dot{B}^{\mathcal{B}}. \qquad (4)$$

Detumbling Control

Many of the detumbling control laws found in the literature are variations of a single control law that is derived from the Lyapunov function

$$V = \frac{1}{2}h^T h. \qquad (5)$$

Taking the time derivative,

$$\dot{V} = h^T \dot{h} = -h^T \hat{B}\mu. \qquad (6)$$

We desire to find μ that minimizes $\dot{V}$ at every instant in time. To do so, we formulate this as an optimization problem with bound constraints that limit the maximum dipole moment the satellite can produce:

$$\begin{aligned} \underset{\mu}{\text{minimize}} \quad & \dot{V} = -h^T \hat{B}\mu \\ \text{subject to} \quad & -\mu_{\max} \leq \bar{\mu} \leq \mu_{\max}. \end{aligned} \qquad (7)$$

This optimization problem is a linear program with a closed-form solution in the form of a bang-bang control law:

$$\mu = \mu_{\max} \, \text{sign}(\hat{h}B), \qquad (8)$$

where the sign function is interpreted element-wise. Bang-bang controllers like (8) are prone to chattering in the presence of noise, so we replace the sign hard saturation with a soft saturation,

$$\mu = \mu_{\max} \tanh(k\hat{h}B), \qquad (9)$$

where the $\tanh$ function is, again, interpreted element-wise and k is a tuning parameter. We refer to this control law as the Lyapunov momentum control law.

The control law in (8) is closely related to the classical B-dot and B-cross control laws [2]. The B-cross law replaces h with ω and relaxes the bang-bang saturation to a linear feedback law with gain k,

$$\mu = k\hat{\omega}B. \qquad (10)$$

Avanzini and Giulietti [5] propose selecting the B-cross controller gain,

$$k = 2\frac{1}{\sqrt{a^3/GM}}(1 + \sin(\xi_m))\lambda_{\min}, \qquad (11)$$

where a is the orbit semi-major axis, GM is the Earth's gravitational parameter, ξ_m is the orbit's geomagnetic inclination and $\lambda_{\min}$ is the minimum eigenvalue of the spacecraft's inertia matrix J.

The B-dot law [4], [1] modifies (10) by making the assumption that

$$\hat{\omega}B \approx -\dot{B}^{\mathcal{B}}, \qquad (12)$$

resulting in

$$\mu = -k\dot{B}^{\mathcal{B}}. \qquad (13)$$

The B-dot law has the advantage that $\dot{B}^{\mathcal{B}}$ is readily estimated from a magnetometer only, so no gyroscope measurements are required for its implementation. However, as $\omega \to 0$, the

approximation in (12) becomes less accurate and the B-dot law suffers from long convergence times.

Desouky [7], [8] presented two control laws: Their "time-optimal" control law is equivalent to (8) and their "B-dot Variant" control law inverts (12) with a regularizing term to solve for ω and substitutes the result into (10) to obtain the control law,

$$\mu = -k\hat{\mathcal{B}}(\epsilon I + \hat{B})^{-1}\dot{B}^{\mathcal{B}}, \tag{14}$$

where $0 < \epsilon \ll 1$, and $\epsilon = 1 \times 10^{-6}$ in practice.

Invernizzi and Lovera [6] use a projection-based method to compute a time-varying gain for an unsaturated version of (8),

$$\mu = k\hat{h}B,$$
$$k = -k_1 \exp\left(-k_2 \frac{B^T J h}{\|B\|(\|h\| + \epsilon)}\right). \tag{15}$$

All of the previously discussed methods are very closely related and suffer from the same fundamental limitation: when the controlled variable (h or ω) and B are aligned their, cross product is zero and the commanded control input goes to zero. The controllers are convergent on long time scales because B is time varying in the orbital frame, so eventually the cross product will no longer be zero. However, they are prone to tracking this uncontrollable subspace, effectively becoming stuck and taking significantly longer to detumble.

Consider the B-cross controller in (10). If we decompose $\omega = \omega^{\|} + \omega^{\perp}$, where $\omega^{\|}$ and $\omega^{\perp}$ are the components of ω parallel and perpendicular to B,

$$\mu = k(\omega^{\|} + \omega^{\perp}) \times B = k\hat{\omega}^{\perp}B, \tag{16}$$

and

$$\dot{h} = -\hat{B}\mu = -k\hat{B}(\hat{\omega}^{\perp}B) = -\lambda\omega^{\perp}, \tag{17}$$

for some $\lambda > 0$. Therefore, h is only reduced in the $\omega^{\perp}$ direction with no change in the $\omega^{\|}$ direction. Figure 1 shows this effect in two simulation runs of the B-cross controller with the same initial conditions and two different gains. At the beginning, the smaller-gain controller decreases $\|h\|$ at a slower rate, but ultimately converges sooner because the larger gain causes the controller to get stuck on the uncontrollable subspace where ω and B are parallel. The smaller gain was chosen based on (11) and the larger gain is a factor of 100 larger. The gain sweep results in Fig. 2 show a similar phenomena occurring with the other controllers. While this phenomenon can be partially mitigated with appropriate tuning, there are no guarantees that the controller will converge without becoming stuck. The result is a longer-than-necessary convergence time and higher-than-necessary energy expenditure.

To address the shortcomings of existing controllers, we relax one of their basic constraints: we derive a controller that does not decrease the angular momentum of the spacecraft monotonically, but still maintains a Lyapunov convergence guarantee *on average*. Intuitively, this allows the controller to trade off increasing the angular momentum instantaneously in exchange for avoiding the uncontrollable subspace and making the angular momentum more controllable in the future.
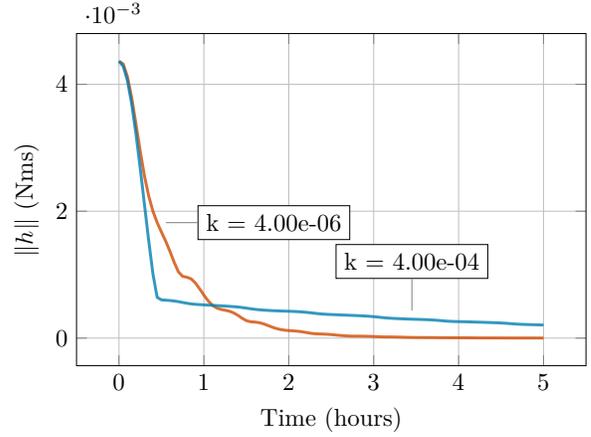

Figure 1: Two simulation runs of the B-cross controller in (10) with different gains. As the gain increases, the controller convergence gets worse because it gets stuck in the uncontrollable subspace where ω and B are parallel.

4. NON-MONOTONIC CONTROLLER DERIVATION

We begin by introducing discrete-time monotonic Lyapunov analysis, then extend it to non-monotonic Lyapunov analysis. The discrete-time dynamical system

$$x_{k+1} = f(x_k) \tag{18}$$

with $x \in \mathbb{R}^n$ has a globally asymptotically stable (GAS) equilibrium at $x = 0$ if there exists a Lyapunov function $V(x) : \mathbb{R}^n \to \mathbb{R}$ such that

$$V(x) > 0 \qquad\qquad \forall x \neq 0 \tag{19a}$$
$$V(0) = 0 \tag{19b}$$
$$V_{k+1} < V_k \qquad\qquad \forall k \tag{19c}$$

where we use the notation $V_k = V(x_k)$. It is well known that there is no general method of finding a Lyapunov function that satisfies (19), even if the system is GAS. Ahmadi and Parrilo suggest that the monotonic decrease condition in (19c) may be too restrictive, and present several alternative stability theorems that only require V to decrease on average [3]. We rely on Theorem 2.1 from their work. It modifies the conditions in (19) so that (18) is GAS at $x = 0$ if there exists a scalar $\alpha \geq 0$ and a Lyapunov function $V : \mathbb{R}^n \to \mathbb{R}$ such that

$$V(x) > 0 \qquad\qquad \forall x \neq 0 \tag{20a}$$
$$V(0) = 0 \tag{20b}$$
$$\alpha(V_{k+2} - V_k) + (V_{k+1} - V_k) < 0 \qquad \forall k. \tag{20c}$$

The condition in (20c) relaxes (19c) to allow V_k to decrease on average between two timesteps.

Non-Monotonic Detumbling

To derive the non-monotonic detumbling controller, we begin with the discrete-time Lyapunov function:

$$V_k = \frac{1}{2}h_k^T h_k. \tag{21}$$

This trivially satisfies (20a) and (20b), so it remains to design the control input μ such that the non-monotonic Lyapunov

3

condition

$$\Delta V = \alpha(V_{k+2} - V_k) + (V_{k+1} - V_k) < 0 \qquad (22)$$

from (20c) is satisfied for $\alpha \geq 0$.

After discretizing the attitude dynamics in time with Euler integration and expanding as shown in the Appendix, we find that

$$\Delta V = \frac{1}{2}\bar{\mu}^T(Q_1 + \alpha Q_2)\bar{\mu} - (q_1 + \alpha q_2)^T\bar{\mu} \qquad (23)$$

where $Q_1, Q_2 \in \mathbb{R}^{6\times 6}$ are symmetric positive semi-definite matrices, $\bar{\mu} \in \mathbb{R}^6 = [\mu_k^T, \mu_{k+1}^T]^T$ is the vector of control inputs at k and $k+1$, and $q_1, q_2 \in \mathbb{R}^6$. This means that ΔV is convex, and, as we will see in the following, its minimum is less than zero. So, it is possible to find $\bar{\mu}$ such that $\Delta V < 0$, and the non-monotonic Lyapunov conditions of (20c) are satisfied.

We wish to find a control law for $\bar{\mu}$ such that ΔV is minimized:

$$\underset{\bar{\mu}}{\text{minimize}} \quad \Delta V = \frac{1}{2}\bar{\mu}^T(Q_1 + \alpha Q_2)\bar{\mu} - (q_1 + \alpha q_2)^T\bar{\mu}$$

$$\text{subject to} \quad -\mu_{\max} \leq \bar{\mu} \leq \mu_{\max}. \qquad (24)$$

Since Q_1, and Q_2 are positive semi-definite, ΔV is not strictly convex and (24) has multiple minima. We add $\frac{1}{2}\beta\bar{\mu}^T\bar{\mu}$ with $1 \gg \beta > 0$ as a regularizing term to make the objective strictly convex. The result is a convex quadratic program that is reliably and quickly solved with a numerical solver. Alternatively, we can make the same simplification as in (9) and solve the unconstrained minimization problem, enforcing a soft saturation constraint on the result. The optimization is then

$$\underset{\bar{\mu}}{\text{minimize}} \quad \begin{aligned} F =& \frac{1}{2}\beta\bar{\mu}^T\bar{\mu} + \frac{1}{2}\bar{\mu}^T(Q_1 + \alpha Q_2)\bar{\mu} \\ & - (q_1 + \alpha q_2)^T\bar{\mu} \end{aligned}. \qquad (25)$$

We find the analytic solution by taking the gradient of F with respect to $\bar{\mu}$ and setting it to zero. The gradient of F is

$$\nabla F = \beta\bar{\mu} + (Q_1 + \alpha Q_2)\bar{\mu} - (q_1 + \alpha q_2). \qquad (26)$$

Setting to zero and solving for $\bar{\mu}$ gives our control law,

$$\bar{\mu}^* = (\beta I + Q_1 + \alpha Q_2)^{-1}(q_1 + \alpha q_2). \qquad (27)$$

We now show that this control law satisfies the nonmonotonic Lyapunov decrease condition. Plugging $\bar{\mu}^*$ into F and recalling that $(I + Q_1 + Q_2)$ is symmetric, we have

$$F^* = -\frac{1}{2}(q_1 + \alpha q_2)^T(\beta I + Q_1 + \alpha Q_2)^{-1}(q_1 + \alpha q_2). \qquad (28)$$

Since $\beta I + Q_1 + \alpha Q_2$ is positive definite, $(\beta I + Q_1 + \alpha Q_2)^{-1}$ is also positive definite, and $F^* < 0$ for all $\alpha, \beta > 0$. The regularizing term in F is always positive in $\bar{\mu}$, so we can conclude that $\Delta V < 0$, which satisfies the nonmonotonic Lyapunov decrease condition in (20c).

Causal Implementation

Examining (40b), we see that the Q_1 and Q_2 matrices in (27) rely on knowledge of B_{k+1}. This is not causal. However, B_{k+1} can be predicted using knowledge of the satellite's orbit and a model of the geomagnetic field. Detumbling is often executed during early operations of a satellite, so orbit knowledge and a computationally expensive geomagnetic field model may not be available. An alternative is to approximate B_{k+1} as

$$B_{k+1} \approx B_k + \Delta t \dot{B}_k^{\mathcal{N}}. \qquad (29)$$

We cannot directly measure $\dot{B}^{\mathcal{N}}$. However, using (4), it can be estimated from multiple magnetometer and gyro measurements.

Complete Controller

Bringing together the development from the last two sections, the discrete non-monotonic controller is given in Algorithm 1. The input B_{k+1} is computed using the approximation in (29). On Lines 1 and 2, we normalize the values of B_* to avoid numerical issues and ensure consistency of performance across the wide range of geomagnetic field magnitudes a spacecraft will experience. Lines 3 to 9 set up the problem components and follow from the derivation in the Appendix. We compute $\bar{\mu}$ on Line 10 by solving a linear system. Finally, on Line 11 we perform a soft saturation of the computed control output and rescale it to satisfy the satellite's control limits.

Algorithm 1: Discrete Non-monotonic controller

Data: Given B_k, B_{k+1}, J, ω, k, α, β
Result: μ

1    $b_1 = B_k/\|B_k\|$
2    $b_2 = B_{k+1}/\|B_{k+1}\|$
3    $\bar{b} = \begin{bmatrix} \hat{b}_1 & \hat{b}_2 \end{bmatrix}$
4    $Z = \beta \begin{bmatrix} I & 0 \\ 0 & 0 \end{bmatrix}$
5    $Q_1 = Z\bar{b}\bar{b}^T Z$
6    $Q_2 = \alpha\bar{b}\bar{b}^T$
7    $h = J\omega$
8    $q_1 = Z\bar{b}h$
9    $q_2 = \alpha\bar{b}h$
10   $\bar{\mu} = (I + Q_1 + Q_2)\backslash(q_1 + q_2)$
11   $\mu = \mu_{\max}\tanh(k\bar{\mu}[1\!:\!3])$

---

5. SIMULATION EXPERIMENTS

All simulations are performed in a 12-degree-of-freedom orbital-and-attitude-dynamics simulation. All code is available on GitHub[1]. The simulation environment relies on the open-source SatelliteDynamics.jl[2] orbital dynamics package and includes perturbations due to J2 and atmospheric drag. The attitude dynamics include orbit-coupled drag torques. To accurately model the geomagnetic field, we use the International Geomagnetic Reference Field (IGRF) [13]. The spacecraft properties used for the simulations are given in Table 1; they reflect the properties for a 1.5U CubeSat with printed circuit board magnetorquers embedded in the solar panels. Noisy sensor measurements and a randomly

---

[1]github.com/RoboticExplorationLab/non-monotonic-detumbling
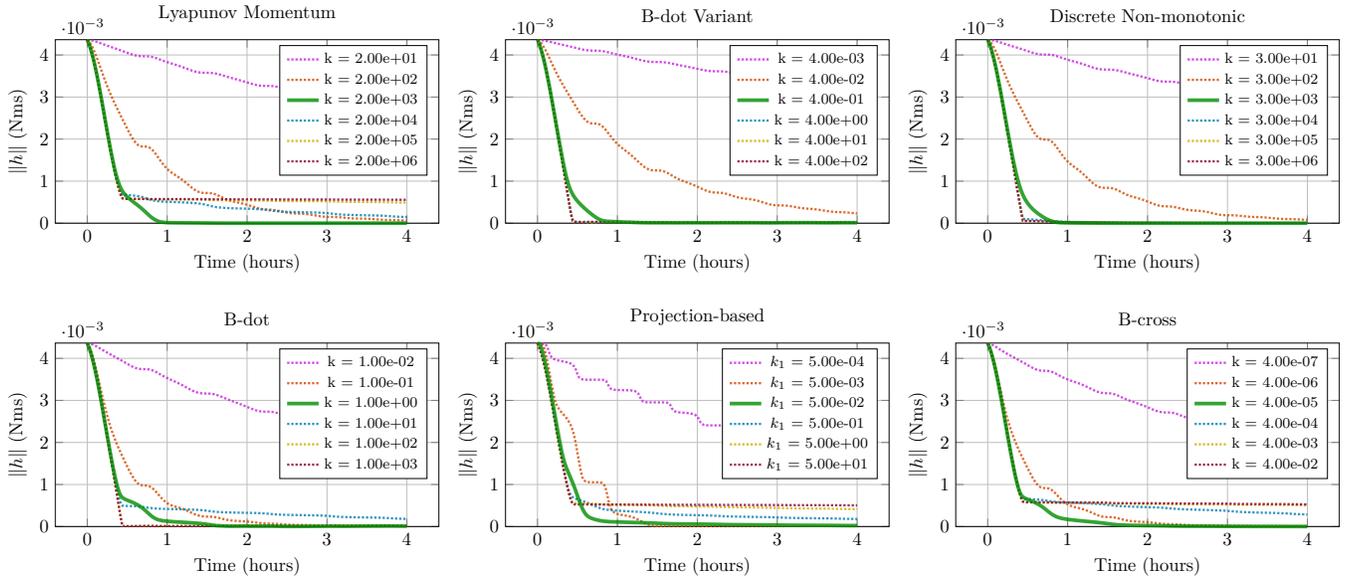[2]sisl.github.io/SatelliteDynamics.jl

Figure 2: Gain sweep study showing the effect each controller's gain has on its detumbling performance for a single initial condition. The solid green line is the gain that was used for the Monte-Carlo simulation experiment shown in Figs. 3 to 5. The other lines are for gains varying from two orders of magnitude lower to three orders of magnitude higher than the chosen gain.
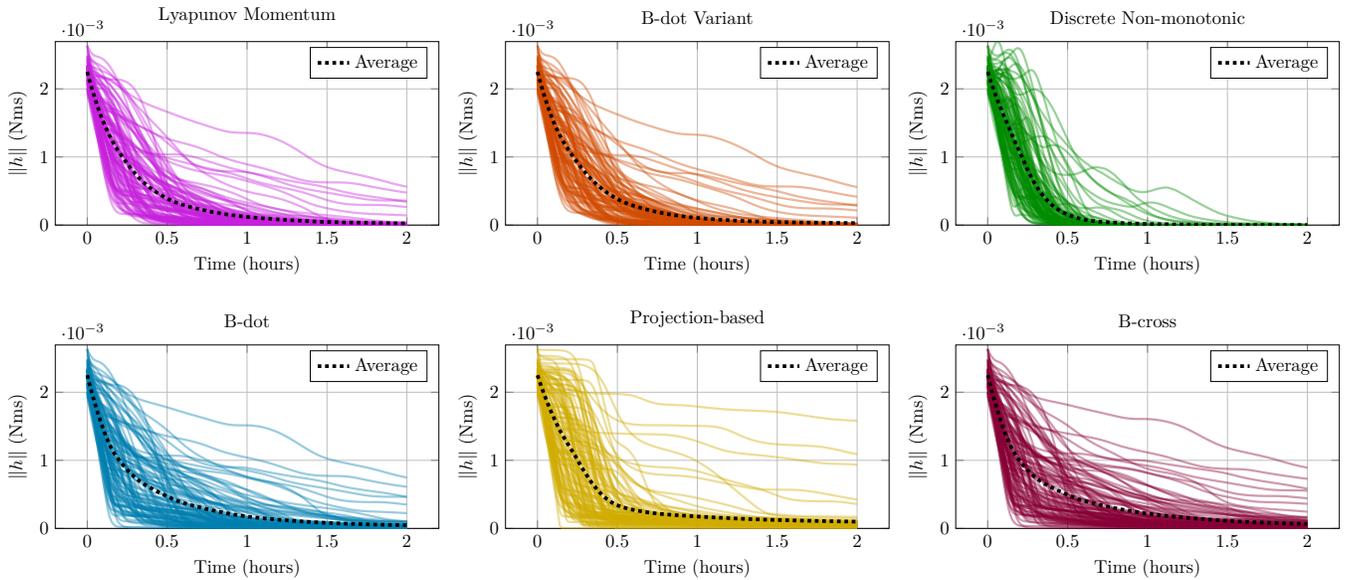

Figure 3: Momentum magnitude versus time plot for each of the controllers discussed in this paper. The Discrete Non-monotonic controller differs from the other controllers in that the system momentum increases before decreasing and converging to zero. This is the key distinction of this controller and allows it to have faster convergence times than other detumbling controllers.

initialized constant gyro bias are also included in the simulation; the noise parameters are representative of low-cost micro-electromechanical (MEMS) gyro and magnetometer hardware.

Each of the controllers is sensitive to its tuning parameter k. To provide meaningful comparisons between controllers, each controller needs to be tuned to perform in the best possible manner. To do so, we simulate the performance impact of each controller's gain, sweeping it over several orders of magnitude. The results of this study are shown in Fig. 2. The solid green line is the gain that was used for the

Monte-Carlo simulation experiment; this gain was chosen as a tradeoff between fast convergence and avoiding high gains that lead to the controller getting stuck in their uncontrollable subspace.

For each controller, the Monte-Carlo simulation starts from each of 100 randomly sampled initial states. Initializing each controller with the same random initial states allows for fair comparison. The ranges and values of the Monte-Carlo initial conditions are sampled uniformly across the ranges given in Table 2. They represent random circular orbits at a fixed altitude and random vehicle axis of rotation with a
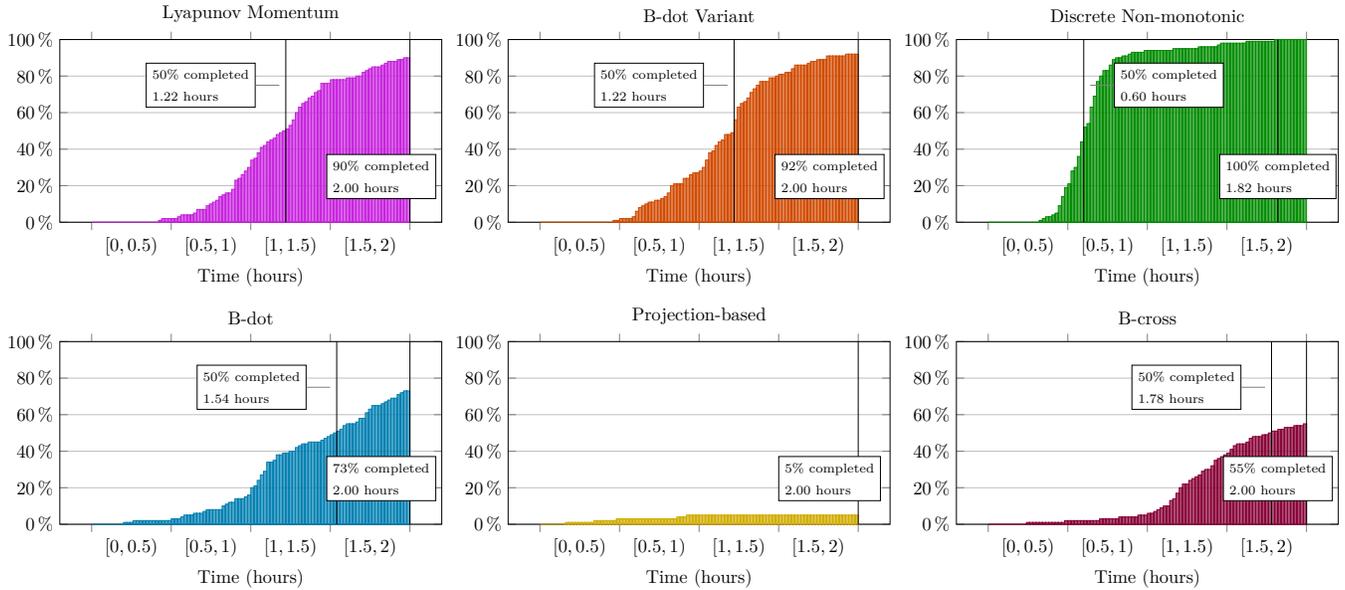
Figure 4: Cumulative distribution of detumble times for each of the controllers discussed in this paper. Detumble times are defined as the time when the satellite first reaches 1% of its initial angular momentum. Each simulation run ended at two hours, so only detumble times less than two hours are counted. Our Discrete Non-monotonic controller has the lowest average detumble time; it is also the only controller to detumble for all simulation runs.
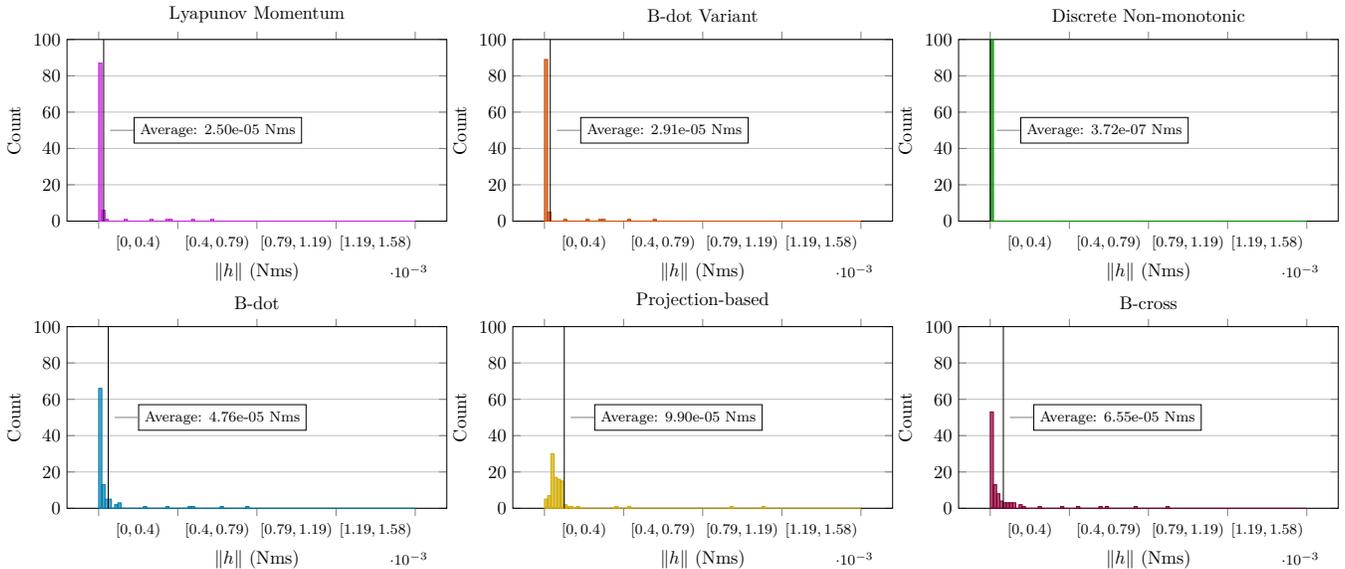

Figure 5: Histogram of final momentum magnitudes for each of the controllers discussed in this paper. Our Discrete Non-monotonic controller is the only controller to have all of its simulation runs in the leftmost bin, with an average final angular momentum that is two orders of magnitude lower than the other controllers.

fixed initial angular velocity magnitude. Since most satellites in low-Earth orbit operate at high inclinations, and to avoid the lack of controllability all magnetorquer control systems experience at near equatorial inclinations [14], we restricted the orbital inclinations to $[20°, 160°)$. The controller parameters and corresponding equation reference are shown in Table 3. In developing this comparison, we attempted to tune all controllers to achieve their best performance.

The simulation results are shown in Figs. 3 to 5. Figure 4 shows a histogram of the time it takes for the spacecraft momentum to be reduced to 1% of its initial value. Many

of the simulation runs of the common control methods do not converge to this 1% threshold within two hours. However, our discrete non-monotonic controller converges within the two hour simulation period for all initial conditions tested, with the majority of the initial conditions converge within one hour. The reason for this can be seen in Fig. 3; it shows the time history of the momentum magnitude for the 100 Monte-Carlo simulation runs, as well as an average time history of these runs. The discrete non-monotonic controller exhibits significantly different behavior than the five other controllers, increasing in momentum one or more times before finally converging to zero. By relaxing the monotonic decrease

requirement for the controller, we have developed a controller that reduces average detumble times by 50% or more.

Figure 5 shows the final angular momentum magnitudes. The discrete non-monotonic controller has converged to a lower angular momentum than the other controllers in all cases. The projection-based controller is particularly susceptible to getting stuck in the uncontrollable subspace and has the worst performance of all of the controllers. The Lyapunov momentum, B-cross, B-dot variant, and B-dot controllers all perform similarly at the beginning of the simulation runs, but the B-cross controller converges significantly slower than the other controllers.

Table 1: Simulated spacecraft properties

Name	Value
Inertia J_{xx}	4.5×10^{-3} kg m^2
J_{xy}	-3.2×10^{-4} kg m^2
J_{xz}	0.0 kg m^2
J_{yy}	5.1×10^{-3} kg m^2
J_{yz}	0.0 kg m^2
J_{zz}	3.7×10^{-3} kg m^2
Mass	1.6 kg
Dimensions	75 cm $\times$ 10 cm $\times$ 15 cm
Drag Coefficient	2.2
$\mu_{\max}$	$[0.070 \quad 0.053 \quad 0.070]$ A m^2
Magnetometer noise	15 nT
Gyro noise	$0.005°/\text{s}/\sqrt{\text{Hz}}$
Gyro bias	$1\,°\,\text{s}^{-1}$

Table 2: Monte-Carlo Initial Condition Distribution

Satellite State	Value
Altitude	400 km
Eccentricity	0
Inclination	$[20°, 160°)$
RAAN	$[0°, 360°)$
Arg. of Latitude	$[0°, 360°)$
$\|\omega\|$	$30°\,\text{s}^{-1}$

Table 3: Controller Parameters

Controller	Parameters
Lyapunonv Momentum (9)	$k = 2.0 \times 10^3$
B-cross (10)	$k = 4.0 \times 10^{-6}$
Discrete Non-monotonic	$k = 3.0 \times 10^3$, $\alpha = 100$,
(Algorithm 1)	$\beta = 1$, $\Delta t = 10$ min
B-dot Variant (14)	$k = 0.4$, $\epsilon = 1 \times 10^{-6}$
Projection-based (15)	$k_1 = 10.0$, $k_2 = 10.0$,
	$\epsilon = 1 \times 10^{-6}$
B-dot (13)	$k = 1.0$

6. CONCLUSIONS

The many variants of B-dot and B-cross controllers in the literature differ primarily in how the controller gains and saturation are selected. Their performance is similar, with each having the potential to get stuck in the uncontrollable subspace where the controlled state (angular momentum or angular velocity) aligns with the magnetic field vector. Even recent magnetorquer detumbling controllers, such as the projection-based controller [6], suffer from this failure mode. The novel non-monotonic Lyapunov magnetorquer detumbling control law we have presented is a more significant departure from the classical B-dot and B-cross control laws: our control law implicitly predicts the future controllability of the system and avoids putting the satellite in an uncontrollable state. In our Monte-Carlo simulations, it achieves detumbling times that are more than twice as fast as the other controllers while operating with realistic sensor noise and gyro bias. In addition, our control law is straightforward to tune and less sensitive to tuning than other control laws.

To put our novel control law into practical use, a high-quality estimate of the time-derivative of the geomagnetic field is needed. Future work will focus on generating this estimate and analyzing the full closed-loop performance of the magnetic field estimator and control law in combination.

APPENDIX

From Section 4, we have

$$\Delta V = \alpha(V_{k+2} - V_k) + (V_{k+1} - V_k) < 0, \qquad (30)$$

and

$$V_k = \frac{1}{2} h_k^T h_k. \qquad (31)$$

Through the rest of this section we drop the subscript k and use $[\cdot]_0 = [\cdot]_k, [\cdot]_1 = [\cdot]_{k+1}, [\cdot]_2 = [\cdot]_{k+2}$ for clarity.

We approximate the discrete time dynamics in (1) using Euler integration, so that

$$h_1 \approx h_0 + \Delta t \dot{h}_0 \qquad (32a)$$
$$= h_0 + \Delta t \tau_0 \qquad (32b)$$
$$= h_0 + \Delta t (\mu_0 \times B_0) \qquad (32c)$$

and

$$h_2 \approx h_1 + \Delta t \dot{h}_1 \qquad (33a)$$
$$= h_0 + \Delta t \tau_0 + \Delta t \tau_1 \qquad (33b)$$
$$= h_0 + \Delta t (\mu_0 \times B_0) + \Delta t (\mu_1 \times B_1). \qquad (33c)$$

Substituting,

$$V_1 = \frac{1}{2} h_1^T h_1 \qquad (34a)$$
$$= \frac{1}{2} \left(h_0^T h_0 + 2\Delta t h_0^T \tau_0 + \Delta t^2 \tau_0^T \tau_0 \right) \qquad (34b)$$

and

$$V_2 = \frac{1}{2} h_2^T h_2 \qquad (35a)$$
$$= \frac{1}{2} \big(h_0^T h_0 + 2\Delta t h_0^T \tau_0 + 2\Delta t h_0^T \tau_1 + \Delta t^2 \tau_0^T \tau_0 $$
$$+ 2\Delta t^2 \tau_0^T \tau_1 + \Delta t^2 \tau_1^T \tau_1 \big) \qquad (35b)$$

so

$$V_1 - V_0 = \frac{1}{2} \left(h_0^T h_0 + 2\Delta t h_0^T \tau_0 + \Delta t^2 \tau_0^T \tau_0 \right)$$
$$- \frac{1}{2} h_0^T h_0 \qquad (36a)$$
$$= \Delta t h_0^T \tau_0 + \frac{1}{2} \Delta t^2 \tau_0^T \tau_0 \qquad (36b)$$
$$= -\Delta t h_0^T \hat{B}_0 \mu_0 + \frac{1}{2} \Delta t^2 \mu_0^T \hat{B}_0^T \hat{B}_0 \mu_0 \qquad (36c)$$

and

$$
\begin{aligned}
V_2 - V_0 &= \frac{1}{2}\big(h_0^T h_0 + 2\Delta t h_0^T \tau_0 + 2\Delta t h_0^T \tau_1 \\
&\quad + \Delta t^2 \tau_0^T \tau_0 + 2\Delta t^2 \tau_0^T \tau_1 + \Delta t^2 \tau_1^T \tau_1\big) \\
&\quad - \frac{1}{2} h_0^T h_0 && \text{(37a)}
\end{aligned}
$$

$$
\begin{aligned}
&= \Delta t h_0^T \tau_0 + \Delta t h_0^T \tau_1 + \frac{1}{2}\Delta t^2 \tau_0^T \tau_0 \\
&\quad + \Delta t^2 \tau_0^T \tau_1 + \frac{1}{2}\Delta t^2 \tau_1^T \tau_1 && \text{(37b)}
\end{aligned}
$$

$$
\begin{aligned}
&= -\Delta t h_0^T \hat{B}_0 \mu_0 \\
&\quad - \Delta t h_0^T \hat{B}_1 \mu_1 \\
&\quad + \frac{1}{2}\Delta t^2 \mu_0^T \hat{B}_0^T \hat{B}_0 \mu_0 && \text{(37c)} \\
&\quad + \Delta t^2 \mu_0^T \hat{B}_0^T \hat{B}_1 \mu_1 \\
&\quad + \frac{1}{2}\Delta t^2 \mu_1^T \hat{B}_1^T \hat{B}_1 \mu_1
\end{aligned}
$$

$$
\text{(37d)}
$$

where we used the identities

$$
\tau = \mu \times B = -B \times \mu = -\hat{B}\mu \tag{38a}
$$

$$
\begin{aligned}
\tau^T \tau &= (\mu \times B)^T (\mu \times B) = (-B \times \mu)^T (-B \times \mu) \\
&= (-\hat{B}\mu)^T (-\hat{B}\mu) = \mu^T \hat{B}^T \hat{B}\mu.
\end{aligned} \tag{38b}
$$

Bringing these terms together, we have

$$
\Delta V \triangleq \alpha(V_2 - V_0) + (V_1 - V_0) \tag{39a}
$$

$$
\begin{aligned}
&= \alpha\big(-\Delta t h_0^T \hat{B}_0 \mu_0 \\
&\quad - \Delta t h_0^T \hat{B}_1 \mu_1 \\
&\quad + \frac{1}{2}\Delta t^2 \mu_0^T \hat{B}_0^T \hat{B}_0 \mu_0 \\
&\quad + \Delta t^2 \mu_0^T \hat{B}_0^T \hat{B}_1 \mu_1 && \text{(39b)} \\
&\quad + \frac{1}{2}\Delta t^2 \mu_1^T \hat{B}_1^T \hat{B}_1 \mu_1\big) \\
&\quad - \Delta t h_0^T \hat{B}_0 \mu_0 \\
&\quad + \frac{1}{2}\Delta t^2 \mu_0^T \hat{B}_0^T \hat{B}_0 \mu_0
\end{aligned}
$$

$$
\begin{aligned}
&= \alpha \frac{1}{2}\Delta t^2 \bar{\mu}^T \bar{B}\bar{B}^T \bar{\mu} \\
&\quad - \alpha \Delta t h_0^T \bar{B}^T \bar{\mu} \\
&\quad + \frac{1}{2}\Delta t^2 \bar{\mu}^T Z \bar{B}\bar{B}^T Z \bar{\mu} && \text{(39c)} \\
&\quad - \Delta t h_0^T \bar{B}^T Z \bar{\mu}
\end{aligned}
$$

$$
\begin{aligned}
&= \frac{1}{2}\bar{\mu}^T Q_1 \bar{\mu} + \frac{1}{2}\alpha \bar{\mu}^T Q_2 \bar{\mu} \\
&\quad - q_1^T \bar{\mu} - \alpha q_2^T \bar{\mu} && \text{(39d)}
\end{aligned}
$$

$$
= \frac{1}{2}\bar{\mu}^T (Q_1 + \alpha Q_2)\bar{\mu} - (q_1 + \alpha q_2)^T \bar{\mu} \tag{39e}
$$

where we defined

$$
\bar{\mu} = \begin{bmatrix} \mu_0 \\ \mu_1 \end{bmatrix} \in \mathbb{R}^{\not{4}}, \tag{40a}
$$

$$
\bar{B} = \begin{bmatrix} \hat{B}_0^T \\ \hat{B}_1^T \end{bmatrix} \in \mathbb{R}^{\not{4} \times \not{\!\!F}} \tag{40b}
$$

$$
Z = \begin{bmatrix} I & 0 \\ 0 & 0 \end{bmatrix} \in \mathbb{R}^{\not{\!\!F} \times \not{\!\!F}} \tag{40c}
$$

$$
Q_1 = \Delta t^2 Z \bar{B}\bar{B}^T Z \tag{40d}
$$

$$
Q_2 = \alpha \Delta t^2 \bar{B}\bar{B}^T \tag{40e}
$$

$$
q_1 = \Delta t (h_0^T \bar{B}^T Z)^T \tag{40f}
$$

$$
q_2 = \alpha \Delta t (h_0^T \bar{B}^T)^T. \tag{40g}
$$

Since $\bar{B}\bar{B}^T$ is symmetric and $\mathrm{rank}(\bar{B}\bar{B}^T) = \mathrm{rank}(\bar{B}) \le 3 < 6$, Q_1 and Q_2 are symmetric and positive semi-definite.

ACKNOWLEDGMENTS

REFERENCES

[1] F. Markley, "Attitude control algorithms for the solar maximum mission," in *Guidance and control conference*, 1978, p. 1247.

[2] F. L. Markley and J. L. Crassidis, *Fundamentals of spacecraft attitude determination and control*. Springer, 2014, vol. 1286.

[3] A. A. Ahmadi and P. A. Parrilo, "Non-monotonic Lyapunov functions for stability of discrete time nonlinear and switched systems," in *2008 47th IEEE conference on decision and control*. IEEE, 2008, pp. 614–621.

[4] A. C. Stickler and K. Alfriend, "Elementary magnetic attitude control system," *Journal of spacecraft and rockets*, vol. 13, no. 5, pp. 282–287, 1976.

[5] G. Avanzini and F. Giulietti, "Magnetic detumbling of a rigid spacecraft," *Journal of guidance, control, and dynamics*, vol. 35, no. 4, pp. 1326–1334, 2012.

[6] D. Invernizzi and M. Lovera, "A projection-based controller for fast spacecraft detumbling using magnetic actuation," *Automatica*, vol. 113, p. 108779, 2020.

[7] M. A. Desouky and O. Abdelkhalik, "A new variant of the B-dot control for spacecraft magnetic detumbling," *Acta Astronautica*, vol. 171, pp. 14–22, 2020.

[8] ——, "Time-optimal magnetic attitude detumbling," *Journal of Spacecraft and Rockets*, vol. 57, no. 3, pp. 549–564, 2020.

[9] R. Wisniewski and F. L. Markley, "Optimal magnetic attitude control," *IFAC Proceedings Volumes*, vol. 32, no. 2, pp. 7991–7996, 1999.

[10] E. Silani and M. Lovera, "Magnetic spacecraft attitude control: a survey and some new results," *Control engineering practice*, vol. 13, no. 3, pp. 357–371, 2005.

[11] A. Gatherer and Z. Manchester, "Magnetorquer-only attitude control of small satellites using trajectory optimization," in *Proceedings of AAS/AIAA Astrodynamics Specialist Conference*, 2019.

[12] M. Y. Ovchinnikov and D. Roldugin, "A survey on active magnetic attitude control algorithms for small satellites," *Progress in Aerospace Sciences*, vol. 109, p. 100546, 2019.

[13] P. Alken, E. Thébault, C. D. Beggan, H. Amit, J. Aubert, J. Baerenzung, T. Bondar, W. Brown, S. Califf, A. Chambodut *et al.*, "International geomagnetic reference field: the thirteenth generation," *Earth, Planets and Space*, vol. 73, no. 1, pp. 1–25, 2021.

[14] S. P. Bhat, "Controllability of nonlinear time-varying systems: applications to spacecraft attitude control using magnetic actuation," *IEEE Transactions on Automatic Control*, vol. 50, no. 11, pp. 1725–1735, 2005.

BIOGRAPHY

Jacob Willis is a PhD candidate in the Robotics Institute at Carnegie Mellon University. He is an NDSEG Fellow and received a BS and MS in Electrical and Computer Engineering from Brigham Young University in 2019 and 2021. His research interests include applications of numerical optimal control for autonomous aerospace systems, with recent work on attitude and formation control of small satellites.

Paulo Fisch is a PhD candidate in the Robotics Institute at Carnegie Mellon University. He has previous experience working at the German Aerospace Center (DLR) and got his Mechanical Engineering degree from the University of São Paulo in 2020. His interests include optimal state estimation for space systems and optimal control, with recent work on satellite orbit determination.

Aleksei Seletskiy is a Junior in Computer Science at Carnegie Mellon Uiversity. His research interests include flight software, state estimation, and optimal control for satellite systems.

Zachary Manchester is an assistant professor in the Robotics Institute at Carnegie Mellon University and founder of the Robotic Exploration Lab. He received a PhD in aerospace engineering in 2015 and a BS in applied physics in 2009, both from Cornell University. His research interests include control and optimization with application to aerospace and robotic systems with challenging nonlinear dynamics.